Modeling Contact Problems Involving Toroidal Surfaces

Filipe Marques[1,2], Mariana Rodrigues da Silva[1,2]

[1] *CMEMS-UMinho, Department of Mechanical Engineering, University of Minho, Campus of Azurém, Guimarães 4804-533 Portugal, fmarques@dem.uminho.pt, m.silva@dem.uminho.pt*

[2] *LABBELS – Associate Laboratory, Braga/Guimarães, Portugal*

Accurately modeling contact interactions in mechanical systems with complex geometries is a critical step towards predicting the dynamic response of the system. In particular, toroidal surfaces are especially challenging in contact mechanics due to their nontrivial geometry involving both convex and concave surfaces, which often results in complex contact interactions when dealing with planar surfaces or other curved bodies. Such shapes frequently appear in several engineering applications, including tires, seals, and various ring components. Hence, the present study focuses on developing a robust and computationally efficient methodology to simulate the contact dynamics between a toroidal surface and a plane by employing a penalty-based compliant force model. This work not only provides a framework for the standalone modeling of toroidal-plane interactions, but also demonstrates broader applicability to systems with more complex surfaces in which some parts can be approximated by toroidal geometry.

The toroidal surface is represented parametrically, involving a set of two angular parameters: one defining the angle along the torus cross-section and another denoting the rotation around the axis of the torus. The proposed procedure facilitates the precise location of points on the torus geometry and enables the use of efficient contact detection methods. Unlike simpler geometries, such as spheres or ellipsoids, the torus requires specialized techniques to accurately identify the contact points and assess pseudo-penetration during contact scenarios. In order to address these challenges, the torus surface is discretized into multiple slices, each treated as a local cylindrical approximation. This slicing approach simplifies the contact region analysis while preserving the geometric fidelity. The interaction between the torus and the plane is evaluated for each slice, and suitable normal and tangential contact force models are adopted. The normal forces are computed using a Hunt and Crossley-based model, which takes into account the properties of the contacting materials, such as stiffness and damping, while the tangential forces are evaluated with a regularized static friction model.

The methodology developed in the context of this work is applied to the dynamic simulation of a generic toroidal body contacting a fixed plane. The obtained results highlight the system's sensitivity to key parameters, including the stiffness and damping of the contact interface and the number of slices utilized to discretize the torus geometry. While increasing the number of slices improves the system's accuracy, it also leads to an increase in the computational cost, imposing a trade-off between precision and efficiency. Additionally, the proposed approach has been able to capture the complex variations in contact regions as the torus orientation changes, showcasing its versatility in handling dynamic scenarios. Future work will focus on refining the model, exploring different contact models, and extending its application to more complex multibody systems. In addition, the extension of this work to supertoroidal shapes is intended.

1. Introduction

Accurate modeling of the contact interactions in mechanical systems with complex geometries is essential for predicting their dynamic behavior, including secondary effects such as deformations, vibrations, friction, and wear. In computational mechanics, and particularly within the framework of multibody dynamics simulations, the mathematical representation of surface geometries plays a crucial role in determining the accuracy and realism of the simulation results. Parametric surface representations are particularly valuable in this context, as they allow for precise and continuous descriptions of three-dimensional shapes without the need to generate excessively detailed mesh-based models. Such formulations are widely utilized in several applications ranging from computer graphics and animation to physical simulations and virtual prototyping [1].

While classical geometric models often rely on simple shapes such as spheres, cylinders, or flat planes, these forms are frequently insufficient to capture the true behavior of components in real-world circumstances. Many engineering problems involve interactions between bodies with more intricate geometries, where oversimplified approximations can lead to significant inaccuracies in both contact detection and force evaluation. Among these more complex surfaces, toroidal geometries are particularly noteworthy due to their prevalence in practical applications [2-5]. Components such as tires, gaskets, seals, and various types of rings or bearings commonly exhibit toroidal features. Their continuous curvature, combining both convex and concave regions, presents unique challenges in the context of contact modeling.

In the framework of multibody dynamics, contact modeling using penalty-based approaches is widely adopted to simulate the interactions between bodies [6-8]. These models impose contact constraints by introducing forces proportional to the interpenetration depth, typically coupled with a damping term to account for energy dissipation. Their popularity is associated with their conceptual simplicity, ease of implementation, and computational efficiency, particularly when contact stiffness is moderate. Such methods have been successfully applied to bodies with various shapes, including spherical, ellipsoidal, and superellipsoidal geometries, with numerous contact scenarios examined in the scientific literature [9-11]. However, despite the practical importance of toroidal surfaces, they have received comparatively less attention over the years, likely due to the increased complexity involved in both contact detection and contact force evaluation.

The primary difficulty lies in the torus's doubly-curved structure, which complicates the accurate determination of contact points, especially when interacting with other curved geometries. Efficient and robust strategies for handling toroidal contacts are therefore essential to guarantee physically meaningful simulations without incurring in excessive computational cost. Moreover, there is a growing need to develop generalized techniques that can scale to more complex surface representations, where toroidal approximations may serve as useful local alternatives.

The present paper addresses these challenges by proposing a physically consistent methodology to simulate the dynamic interaction between a toroidal surface and a planar surface. A parametric representation of the torus is adopted, allowing for precise localization of surface points. The torus is discretized into a set of slices, each approximated locally as a cylindrical patch, facilitating efficient contact detection and force evaluation. A Hunt and Crossley-based model is employed for the computation of normal contact forces, while tangential interactions are modeled using a regularized friction law.

The remainder of this paper is organized as follows. Section 2 presents the mathematical formulation of the toroidal surface geometry. Section 3 describes the proposed methodology for contact detection and contact force evaluation. Section 4 demonstrates the approach through numerical simulations and discusses the influence of key parameters. Finally, Section 5 summarizes the main conclusions and outlines directions for future work.

2. Toroidal Geometry Definition

A torus is a three-dimensional geometric surface generated by the revolution of a circle around an axis that lies in the same plane as the circle but does not intersect it. This operation results in a closed surface with axial symmetry, commonly visualized as a ring-shaped object. The geometry of a torus is characterized by two radii, the major radius, R, which represents the distance from the axis of rotation to the center of the circle, and the minor radius, r, which corresponds to the radius of the revolving circle. The implicit form of the torus surface, defined in a local reference system (ξ_T, η_T, ζ_T), and represented in Figure 1, can be written as

$$F\left(\xi_T, \eta_T, \zeta_T\right) = \left(\frac{\sqrt{\xi_T^{\,2} + \eta_T^{\,2}} - R}{r}\right)^2 + \left(\frac{\zeta_T}{r}\right)^2 - 1 = 0 \tag{1}$$

Note that this implicit formulation assumes the axis of revolution is aligned with the ζ_T axis of the local coordinate system, and that the center of the torus lies at the origin of that coordinate system (see Figure 1).

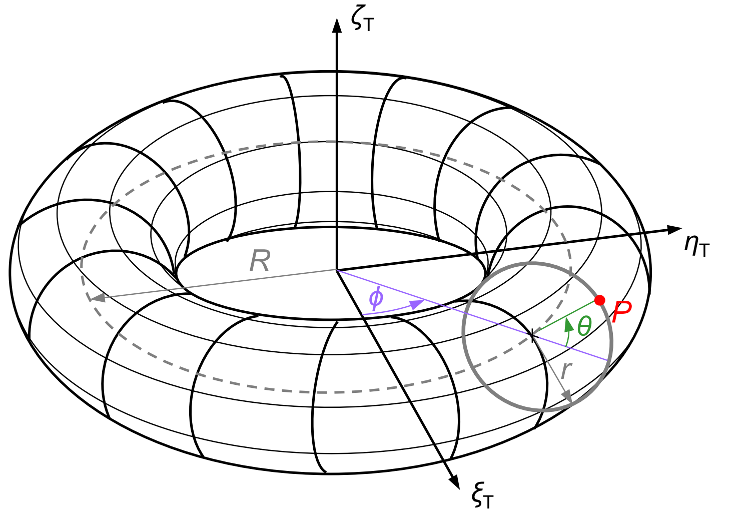

Figure 1: General representation of a torus surface.

In order to fully define the position and orientation of the torus surface, which belongs to a given body i, in the three-dimensional space in a general case, it is required to specify the location of the torus center and the unit vector along the axis of revolution, $\mathbf{v}_i$, which coincides with the ζ_T local axis. This generalization of the location and orientation of the torus significantly complicates the use of the implicit surface formulation. Moreover, this representation is not convenient for the contact detection methodology adopted in the context of this work.

Instead, the torus surface can be treated as a parametrized surface, in which any point P located at that surface can be fully described by a set of two angular parameters, that is, θ defines the angle along the circular cross-section and ϕ denotes the rotation around the axis of the torus, as depicted in Figure 1. Based on these parameters the location of the point P in the torus local coordinate system can be defined as

$$\mathbf{s}''_{\mathrm{T},P}\left(\phi_P,\theta_P\right)=\begin{Bmatrix}\left(R+r\cos\theta_P\right)\cos\phi_P\\ \left(R+r\cos\theta_P\right)\sin\phi_P\\ r\sin\theta_P\end{Bmatrix} \tag{2}$$

where, θ_P and ϕ_P represent the angular parameters corresponding to point P.

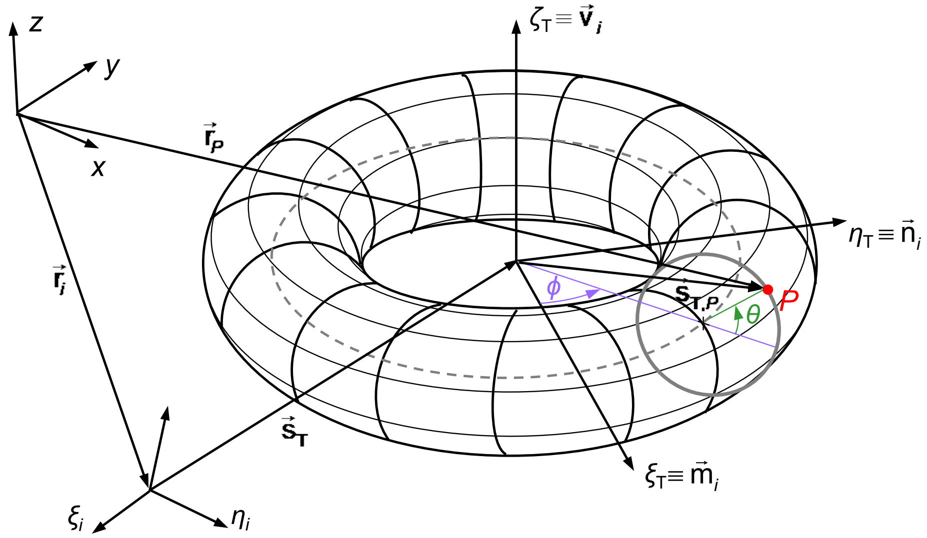

Figure 2: Representation of the location of an arbitrary point P on the torus surface.

Having this in mind, and following the representation of Figure 2, the location of point P on the torus surface that belongs to body i, can be established in global coordinates as

$$\mathbf{r}_P=\mathbf{r}_i+\mathbf{s}_\mathrm{T}+\mathbf{s}_{\mathrm{T},P} \tag{3}$$

in which $\mathbf{r}_i$ is the vector defining the location of the body i reference frame in global coordinates, $\mathbf{s}_{\mathrm{T}}$ represents the location of the torus center with respect to body i reference system in global coordinates, and $\mathbf{s}_{\mathrm{T},P}$ denotes the location of point P with respect to the torus center in global coordinates and can be expressed by

$$\mathbf{s}_{\mathrm{T},P} = \mathbf{A}_i \mathbf{A}_{\mathrm{T}} \mathbf{s}''_{\mathrm{T},P} \tag{4}$$

where $\mathbf{A}_i$ is the transformation matrix associated with body i reference system, and $\mathbf{A}_{\mathrm{T}}$ denotes the transformation matrix from the torus local reference system to the body i coordinate system which can be defined as

$$\mathbf{A}_{\mathrm{T}} = \begin{bmatrix} \mathbf{m}_i & \mathbf{n}_i & \mathbf{v}_i \end{bmatrix} \tag{5}$$

where $\mathbf{m}_i$, $\mathbf{n}_i$ and $\mathbf{v}_i$ denote unit vectors along the ξ_{T}, η_{T} and ζ_{T} directions, respectively, in body i local coordinates.

Since the position of an arbitrary point is parametrized, it is possible to analytically derive the expressions for the tangent and normal vectors at that point. These vectors are especially useful in the contact detection process and in the correct application of contact forces. The tangent vectors, depicted in Figure 3, can be obtained in the torus local coordinate system by computing the partial derivatives of Eq. (2) as

$$\mathbf{s}''_{\theta} = \frac{\partial \mathbf{s}''_{\mathrm{T},P}}{\partial \theta} = \begin{Bmatrix} -r\cos\phi_P \sin\theta_P \\ -r\sin\phi_P \sin\theta_P \\ r\cos\theta_P \end{Bmatrix} \tag{6}$$

$$\mathbf{s}''_{\phi} = \frac{\partial \mathbf{s}''_{\mathrm{T},P}}{\partial \phi} = \begin{Bmatrix} -\left(R + r\cos\theta_P\right)\sin\phi_P \\ \left(R + r\cos\theta_P\right)\cos\phi_P \\ 0 \end{Bmatrix} \tag{7}$$

and, hence, transformed into tangent unit vectors as

$$\mathbf{t}''_{\theta,P} = \frac{\mathbf{s}''_{\theta}}{\left\|\mathbf{s}''_{\theta}\right\|} = \begin{Bmatrix} -\cos\phi_P \sin\theta_P \\ -\sin\phi_P \sin\theta_P \\ \cos\theta_P \end{Bmatrix} \tag{8}$$

$$\mathbf{t}''_{\phi,P} = \frac{\mathbf{s}''_{\phi}}{\left\|\mathbf{s}''_{\phi}\right\|} = \begin{Bmatrix} -\sin\phi_P \\ \cos\phi_P \\ 0 \end{Bmatrix} \tag{9}$$

Then, the normal unit vector of the torus surface at point P can be calculated as

$$\mathbf{n}''_{P} = \tilde{\mathbf{t}}''_{\phi,P}\mathbf{t}''_{\theta,P} = \begin{Bmatrix} \cos\phi_P \cos\theta_P \\ \sin\phi_P \cos\theta_P \\ \sin\theta_P \end{Bmatrix} \tag{10}$$

These vectors can be expressed in the global coordinate system by pre-multiplying Eqs. (8)-(10) by the transformation matrix $\mathbf{A}_i\mathbf{A}_{\mathrm{T}}$.

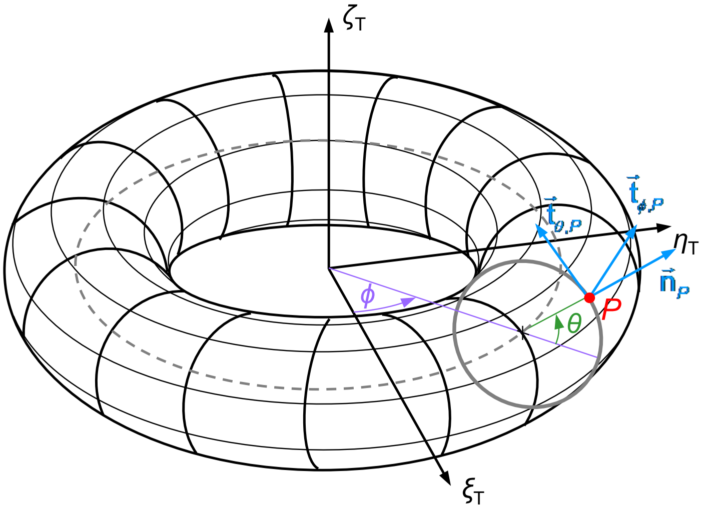

Figure 3: Representation of the normal and tangent vectors to the torus surface.

3. Contact Modeling

The methodology adopted in this work to model the contact between toroidal and planar surfaces is based on a regularized approach, in which the contact interaction is treated as a continuous process. In this context, the bodies are allowed to locally deform, which is quantified through the computation of a pseudo-penetration between the undeformed geometries. Accordingly, a methodology to estimate the pseudo-penetration and locate the contact points is required to accurately determine both the direction and magnitude of the resulting contact forces.

Having that in mind, given the geometric complexity of the torus, which contains both convex and concave regions, its surface is divided into N_s equally-sized slices to facilitate the contact detection process. Hence, the contact is checked between each slice s of the torus belonging to a given body i and the planar surface of body j, as schematized in Figure 4. While the torus is defined by its two radii, the position of its center, the unit vector along its symmetry axis and the number of slices, the planar surface can be simply defined by any point P_j on the plane and its normal unit vector, $\mathbf{n}_\mathrm{P}$.

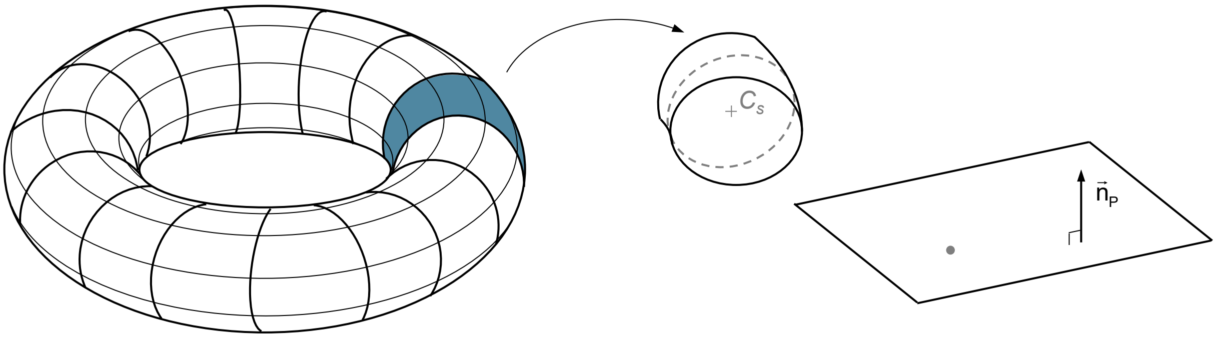

Figure 4: Schematic representation of the torus discretization and contact detection methodology.

In this framework, the total contact force is assumed to be the sum of the individual contact forces developed at each contacting slice. The penetration for each slice is evaluated by analyzing the intersection between the circumference that describes its middle section and the plane. The center of the slice s, denoted by point C_s, is defined through the angular parameter, ϕ_s, which denotes the rotation around the axis of the torus, as

$$\mathbf{r}_i^{C_s} = \mathbf{r}_i + \mathbf{s}_\mathrm{T} + \mathbf{A}_i\mathbf{A}_\mathrm{T}\begin{Bmatrix} R\cos\phi_s \\ R\sin\phi_s \\ 0 \end{Bmatrix} \tag{11}$$

In order to help promote the contact detection process, the normal vector of the plane is projected onto the plane that contains the middle section of the torus slice. Hence, the normal vector to this middle section must be computed. From the observation of Figure 3, it can be concluded that this vector coincides with the tangent vector in the ϕ direction given by Eq. (9) and denoted as $\mathbf{t}_{\phi,s}$. Finally, the normal unit vector, $\mathbf{n}_\mathrm{P}$, projected onto the middle section plane can be estimated as

$$\mathbf{n}_{\mathrm{P},s} = \mathbf{n}_\mathrm{P} - \mathbf{n}_\mathrm{P}^\mathrm{T}\mathbf{t}_{\phi,s}\mathbf{t}_{\phi,s} \tag{12}$$

Using this vector, the location of the potential contact point on the middle section of the slice s, $Q_{i,s}$ can be determined by subtracting the torus radius in that direction from the center point as

$$\mathbf{r}_i^{Q_s} = \mathbf{r}_i^{C_s} - r\frac{\mathbf{n}_{\mathrm{P},s}}{\left\|\mathbf{n}_{\mathrm{P},s}\right\|} \tag{13}$$

Then, the distance between this point and the contacting plane can be computed as

$$d_s = \mathbf{n}_\mathrm{P}^\mathrm{T}\left(\mathbf{r}_i^{Q_s} - \mathbf{r}_j^P\right) \tag{14}$$

where $\mathbf{r}_j^P$ represents the location of point P on the plane belonging to body j in global coordinates. The evaluation of Eq. (13) allows to determine if there is penetration between the slice s and the plane. If d_s is positive, the corresponding slice does not contact the plane. In turn, if d_s holds a negative value, penetration exists with equal magnitude (δ_s = - d_s). In that case, the location of the corresponding contact point on the planar surface, $Q_{j,s}$, can be calculated as

$$\mathbf{r}_j^{Q_s} = \mathbf{r}_i^{Q_s} + \delta_s\mathbf{n}_\mathrm{P} \tag{15}$$

Once the location of the contact points is known, their global velocities can be computed, which are necessary to estimate the penetration velocity for each slice s as follows

$$\dot{\delta}_s = \left(\dot{\mathbf{r}}_j^{Q_s} - \dot{\mathbf{r}}_i^{Q_s}\right)^{\mathrm{T}} \mathbf{n}_{\mathrm{P}} \tag{16}$$

where $\dot{\mathbf{r}}_i^{Q_s}$ and $\dot{\mathbf{r}}_j^{Q_s}$ denote the linear velocity of the contact points on the torus and the plane, respectively. In a similar way, the relative tangential velocity between contact points can be evaluated as

$$\mathbf{v}_{\mathrm{t},s} = \dot{\mathbf{r}}_j^{Q_s} - \dot{\mathbf{r}}_i^{Q_s} - \dot{\delta}_s \mathbf{n}_{\mathrm{P}} \tag{17}$$

These kinematic quantities are required for the subsequent computation of the contact forces. In what concerns the normal force, a Hertzian-based contact force model is considered in this work. Specifically, the classical Hertzian contact law is extended with the addition of a damping term to represent viscoelastic behavior, accounting for energy dissipation without assuming permanent deformation. Hunt and Crossley [12] were the precursors in this modeling approach and proposed describing the normal force in the following form

$$f_{\mathrm{n}} = k\delta^n + \chi\delta^n\dot{\delta} \tag{18}$$

where k is the contact stiffness, n is an exponent that defines the degree of nonlinearity, and χ is the hysteresis damping factor. This damping term has been the subject of extensive research during the past decades [13, 14], and it commonly based on the estimation of the initial impact velocity. That feature makes extremely important to determine the exact instant in which the contact begins, requires a careful handling of the impact velocity values when dealing with variable time step and multiple contacts, and starts to lose meaning for long continuous contacts. These drawbacks may complicate the implementation of the contact model and create numerical problems. To avoid these issues, a constant hysteresis damping factor is considered in this work as

$$f_{\mathrm{n}} = k\delta^n\left(1+\bar{\chi}\dot{\delta}\right) \qquad \text{where} \qquad \bar{\chi} = \frac{\chi}{k} \tag{19}$$

It must be noted that the previous expression must be employed to calculate the normal force contribution for each slice using the corresponding kinematic quantities. In order to estimate the contact stiffness, the torus slice is approximated by a cylindrical segment [15], which is a reasonable assumption when the number of slices is sufficiently large. Accordingly, the normal stiffness is defined based on the elastic foundation theory, which treats the contact as volume supported by an array of independent distributed springs. In this way, the normal contact force developed in slice s is computed as

$$f_{\mathrm{n},s} = \frac{E^*\sqrt{2rL_s}}{h}\delta_s^{\,3/2}\left(1+\bar{\chi}\dot{\delta}_s\right) \tag{20}$$

in which h is the characteristic depth of the elastic foundation contributing to normal contact stiffness, L_s denotes the length of the contacting cylinder, i.e., the slice thickness which depends on the level of discretization, and E^* represents the composite modulus of the two colliding bodies, which can be calculated as

$$E^* = \left(\frac{1-\nu_i^2}{E_i} + \frac{1-\nu_j^2}{E_j}\right)^{-1} \tag{21}$$

where E_i and E_j correspond to the Young's moduli, and ν_i and ν_j express the Poisson's ratios of bodies i and j, respectively.

Since Eq. (20) provides the magnitude of the normal force only, its vector form can be expressed as

$$\mathbf{f}_{\mathrm{n},s} = f_{\mathrm{n},s}\mathbf{n}_{\mathrm{P}} \tag{22}$$

Regarding the tangential contact forces, it is assumed that there is dry frictional contact between both contacting surfaces. Bearing that in mind, a continuous static friction model is utilized here [16], in which the Coulomb friction is considered. In order to avoid numerical issues associated with the discontinuity of friction force when the relative tangential velocity is close to zero, a regularized approach is adopted to smooth that transition. The tangential force can be computed as

$$\mathbf{f}_{\mathrm{t},s} = f_{\mathrm{C},s}\tanh\left(k_{\mathrm{t}}\left\|\mathbf{v}_{\mathrm{t},s}\right\|\right)\mathrm{sgn}\left(\mathbf{v}_{\mathrm{t},s}\right) \tag{23}$$

where k_{t} defines the slope of the friction curve near zero velocity, and $f_{\mathrm{C},s}$ denotes the magnitude of Coulomb friction for slide s, given by

$$f_{\mathrm{C},s} = \mu_{\mathrm{k}} f_{\mathrm{n},s} \tag{24}$$

in which μ_{k} represents the kinetic coefficient of friction.

Finally, the contact forces determined by Eqs. (22) and (23) must be applied at the contact points identified in Eqs. (13) and (15). These forces are then included as external forces in the Newton-Euler equations of motion for the multibody mechanical system to which torus-plane contact belongs.

4. Example of Application

In order to demonstrate the effectiveness of the proposed methodology, an example of application is presented in this section. A simple multibody system without any kinematic constraints is considered, i.e., a free-falling torus impacting a fixed horizontal plane, as illustrated in Figure 5. In this context, two cases are analyzed: one in which the torus's reference frame is aligned with the plane's reference system (see Figure 5a), and another where the torus is rotated 60º around the x-axis (see Figure 5b).

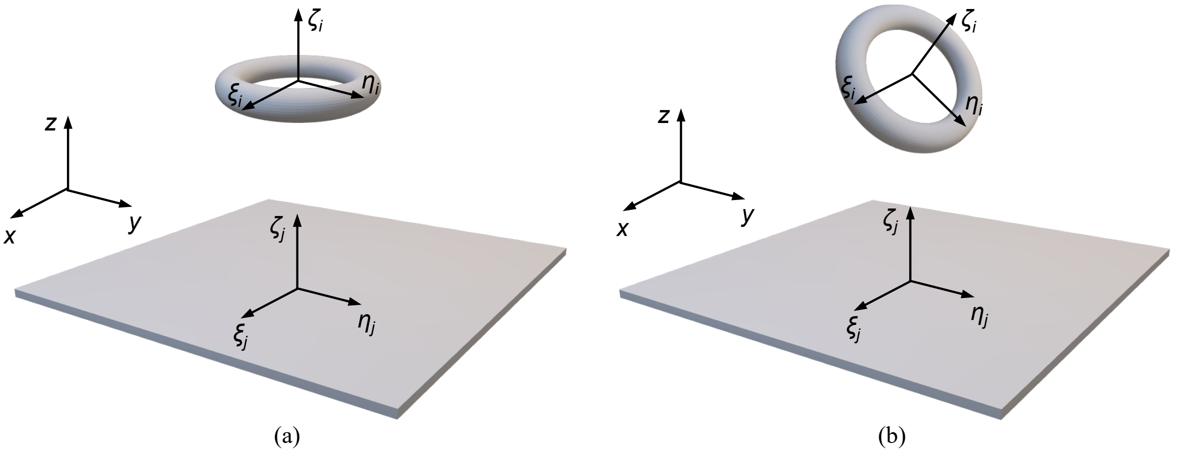

Figure 5: Representation of the simulated application cases: (a) free-falling torus starting from a horizontal position, and (b) free-falling torus starting with a 60º rotation.

In the first configuration, the torus maintains a perfect alignment with the plane, resulting in an uniform contact where all slices simultaneously impact the plane, and frictional forces are negligible. In contrast, the second configuration introduces a more generic and realistic contact scenario, where the inclination of the torus induces uneven contact and promotes the development of frictional effects.

In both cases, the initial position of the center of mass of the torus is 50 mm above the plane. The time integration of the equations of motion is performed using a variable time-step scheme with MATLAB's ode15s solver, with a reporting time step of 10^{-5} s. The total simulation time is 1 s. The geometrical and material properties used in the simulations are summarized in Table 1, while the contact model parameters are listed in Table 2.

Table 1: Material and geometrical properties considered in the simulations.

Property	Value
Torus Major Radius, R	25 mm
Torus Minor Radius, r	5 mm
Torus Mass	9.68×10^{-2} kg
Torus Mass Moment of Inertia, $I_{\xi\xi}$	3.90×10^{-5} kg·m^2
Torus Mass Moment of Inertia, $I_{\eta\eta}$	3.90×10^{-5} kg·m^2
Torus Mass Moment of Inertia, $I_{\zeta\zeta}$	6.23×10^{-5} kg·m^2
Torus Young's Modulus, E_i	210 GPa
Torus Poisson Ratio, ν_i	0.3
Plane Young's Modulus, E_j	10 GPa
Plane Poisson Ratio, ν_j	0.3

Table 2: Parameters selected for the developed contact methodology .

Property	Value
Number of Slices, N_s	36
Force exponent, n	1.50
Characteristic depth, h	1.00 m
Hysteresis Damping Factor, $\bar{\chi}$	0.05
Slope of friction curve, k_t	1000 s/m
Kinetic Coefficient of Friction, μ_k	0.20

For the first simulation case, corresponding to a horizontally aligned free-falling torus, the uniform contact condition causes all slices to contact the plane simultaneously, leading to purely vertical motion. Consequently, frictional forces were neglected by setting the coefficient of friction to zero. This scenario was tested with different values for the hysteresis damping factor to evaluate its effect on energy dissipation. As shown in Figure 6a, the proposed methodology ensures energy conservation when the damping factor is set to zero. Furthermore, the results presented in Figure 6 demonstrate that the methodology produces stable and consistent behavior across the different damping values tested. This is evidenced by the regular oscillation of the torus height after each impact, with a consistent level of energy loss that reflects the selected damping factor.

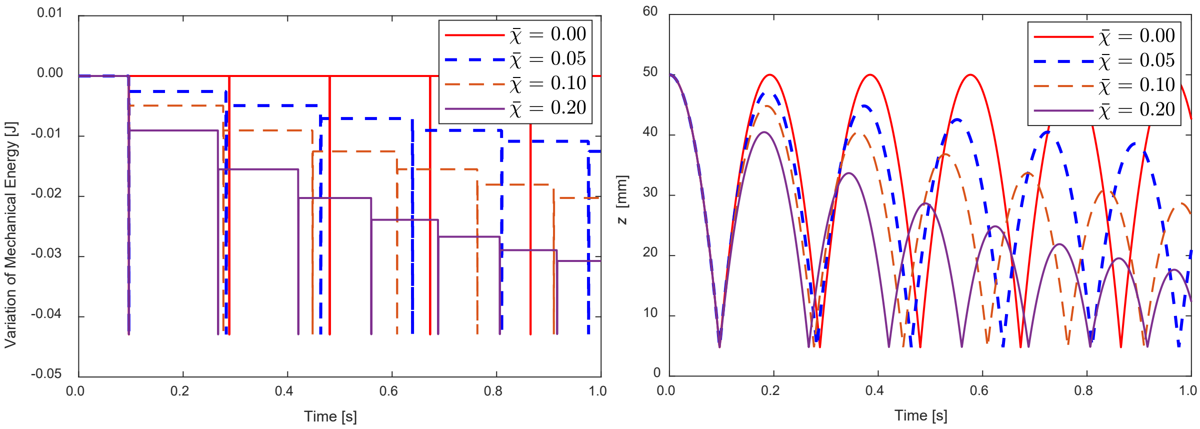

(a) (b)

Figure 6: Results for the first simulation scenario with different damping factors: (a) variation of mechanical energy, and (b) vertical position of the torus center of mass.

For the second simulation case, involving a torus falling with an initial angle of 60º relative to the plane, the trajectory of the center of mass of the torus is displayed in Figure 7a, in which 36 slices were considered. The initial position is marked in blue and gradually transitions to red as time progresses towards the final position. The time interval between two consecutive points on the plot is 2 ms. This scenario was simulated using different numbers of slices to discretize the torus surface, starting with 9 slices and doubling the number successively up to 144 slices (see Figures 7b, 7c and 7d). The computational cost associated with each discretization level is shown in Figure 8, where the CPU time ratio is compared across all cases.

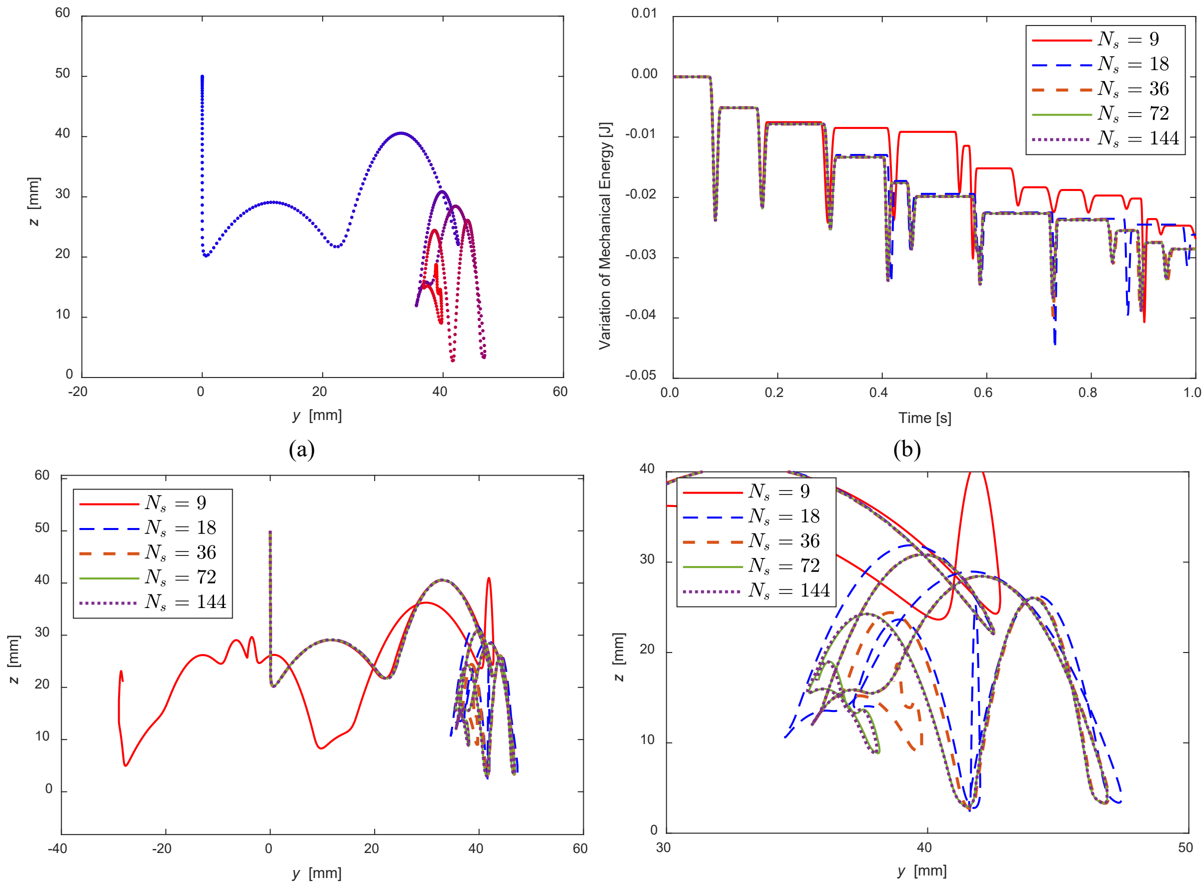

Figure 7: Results for the second simulation scenario: (a) trajectory of the torus center of mass, (b) variation of mechanical energy for different number of slices, (c) trajectory of the torus center of mass for different number of slices, and (d) zoomed view of trajectory of the torus center of mass.

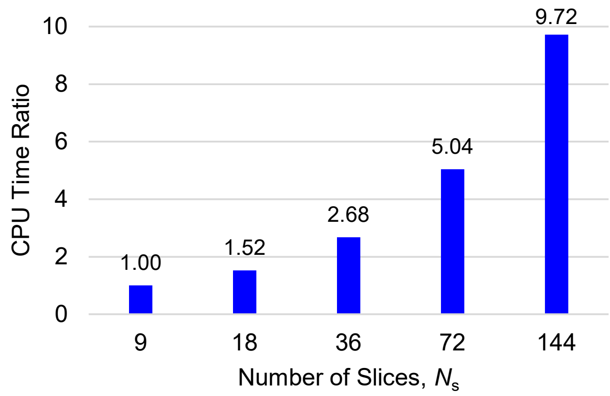

Figure 8: CPU time ratio of the simulations performed with different number of slices.

The results indicate a direct and clear influence of the number of slices on the computational cost. Although the increase in CPU time is not strictly proportional to the increase in the number of slices, a strong correlation is evident. While fewer slices significantly reduce computation time, the results also show that it may lead to unstable or inaccurate dynamic behavior, as demonstrated by the divergence observed in the case with 18 slices and, more significantly, in the case with 9 slices. As shown in Figures 7c and 7d, beyond a certain number of slices, further increasing the discretization does not yield substantial improvements in the dynamic response, suggesting the existence of an optimal balance between accuracy and computational efficiency.

5. Concluding Remarks

In this work, a new methodology was proposed for modeling contact interactions between toroidal and planar surfaces within a multibody dynamics framework. The approach relies on a regularized contact force model based on pseudo-penetration evaluation, employing a parametric representation of the torus and a slicing strategy to simplify contact detection and force computation. A Hunt and Crossley-based normal force model, combined with a regularized Coulomb friction law for tangential interactions, was adopted to simulate the dynamic response of contacting bodies. The complete formulation for point localization, surface parametrization, tangent and normal vector evaluation, and contact force computation was presented in detail.

Preliminary application cases involving the free fall of a torus impacting a plane were simulated to demonstrate the potential and effectiveness of the developed methodology. The results highlighted the model's capability to produce stable dynamic responses for different contact configurations and discretization levels. Although the initial results are promising, further testing is required to fully assess the robustness of the approach, particularly under more complex contact scenarios involving higher impact velocities, rolling contacts, and multiple bodies. Future work will focus on expanding the range of applications to more general and challenging cases.

6. References

[1] Barr, A. H., "Superquadrics and Angle-Preserving Transformations", *IEEE Computer Graphics and Applications* 1(1), 11-23 (1981)

[2] Hu, Y., Zhu, J., "Computed tomography simulation using supertoroids", *Journal of X-Ray Science and Technology* 18(1), 1-13 (2010)

[3] Hatch H.W., McCann G.W., "Tabular Potentials for Monte Carlo Simulation of Supertoroids with Short-Range Interactions", *Journal of Research of the National Institute of Standards and Technology* 124, 124032 (2019)

[4] G. Agúndez, A., García-Vallejo, D., Freire, E., "Analytical and numerical stability analysis of a toroidal wheel with nonholonomic constraints", *Nonlinear Dynamics* 112(4), 2453-2476 (2024)

[5] Millan, P., Ambrósio, J., "Tire–road contact modelling for multibody simulations with regularised road and enhanced UA tire models", *Multibody System Dynamics* 63(1), 104891, 273-302 (2025)

[6] Skrinjar, L., Slavič, J., Boltežar, M., "A review of continuous contact-force models in multibody dynamics", *International Journal of Mechanical Sciences* 145, 171-187 (2018)

[7] Corral, E., Moreno, R.G., García, M.J.G., Castejón, C., "Nonlinear phenomena of contact in multibody systems dynamics: a review" *Nonlinear Dynamics* 104(2), 1269-1295 (2021)

[8] Flores, P., "Contact mechanics for dynamical systems: a comprehensive review", *Multibody System Dynamics* 54(2), pp. 127–177, 2022.

[9] Lopes, D.S., Silva, M.T., Ambrósio, J.A., Flores, P., “A mathematical framework for rigid contact detection between quadric and superquadric surfaces”, *Multibody System Dynamics* 24(3), 255-280 (2010)

[10] Ambrósio, J., “A general formulation for the contact between superellipsoid surfaces and nodal points”, *Multibody System Dynamics* 50(4), 415-434 (2020)

[11] Corral, E., Moreno, R.G., Meneses, J., García, M.J.G., Castejón, C., “Spatial algorithms for geometric contact detection in multibody system dynamics”, *Mathematics* 9(12), 1359 (2021)

[12] Hunt, K.H., Crossley, F.R.E., “Coefficient of restitution interpreted as damping in vibroimpact”, *Journal of Applied Mechanics, Transactions ASME* 42(2), 440-445 (1975)

[13] Rodrigues da Silva, M., Marques, F., Tavares da Silva, M., Flores, P., “A compendium of contact force models inspired by Hunt and Crossley's cornerstone work” *Mechanism and Machine Theory* 167, 104501 (2022)

[14] Poursina, M., Nikravesh, P.E., “A new model with uniform damping force for frictionless impacts with non-permanent deformation at the time of separation”, *Multibody System Dynamics* 63(1), 04017, 235-253 (2025)

[15] Pereira, C.M., Ramalho, A.L., Ambrósio, J.A., “A critical overview of internal and external cylinder contact force models”, *Nonlinear Dynamics* 63(4), 681-697 (2011)

[16] Marques, F., Flores, P., Pimenta Claro, J.C., Lankarani, H.M., “A survey and comparison of several friction force models for dynamic analysis of multibody mechanical systems”, *Nonlinear Dynamics* 86(3), 1407-1443 (2016)